Calibration of the comprehensive NDHA-N2O dynamics model for nitrifier-enriched biomass using targeted respirometric assays

Domingo-Felez, Carlos; Calderó-Pascual, María; Sin, Gürkan; Plósz, Benedek G.; Smets, Barth F.

Published in:
Water Research

Link to article, DOI:
10.1016/j.watres.2017.09.013

Publication date:
2017

Document Version
Peer reviewed version

Title

Calibration of the comprehensive NDHA-N_2O dynamics model for nitrifier-enriched biomass using targeted respirometric assays.

Author list

Carlos Domingo-Félez[a], María Calderó-Pascual[a], Gürkan Sin[b], Benedek G. Plósz[a,1], Barth F. Smets[a]*

[a]Department of Environmental Engineering, Technical University of Denmark, Miljøvej 115, 2800 Kgs. Lyngby, Denmark

[b]Department of Chemical and Biochemical Engineering, Technical University of Denmark, Søltofts Plads 227, 2800 Kgs. Lyngby, Denmark

[1]Present address: Department of Chemical Engineering, University of Bath, Bath, England.

* Corresponding author:

Barth F. Smets, Phone: +45 4525 1600, Fax: +45 4593 2850, E-mail: bfsm@env.dtu.dk

Abstract

The NDHA model comprehensively describes nitrous oxide (N_2O) producing pathways by both autotrophic ammonium oxidizing and heterotrophic bacteria. The model was calibrated via a set of targeted extant respirometric assays using enriched nitrifying biomass from a lab-scale reactor. Biomass response to ammonium, hydroxylamine, nitrite and N_2O additions under aerobic and anaerobic conditions were tracked with continuous measurement of dissolved oxygen (DO) and N_2O.

The sequential addition of substrate pulses allowed the isolation of oxygen-consuming processes. The parameters to be estimated were determined by the information content of the datasets using identifiability analysis. Dynamic DO profiles were used to calibrate five parameters corresponding to endogenous, nitrite oxidation and ammonium oxidation processes. The subsequent N_2O calibration was not significantly affected by the uncertainty propagated from the DO calibration because of the high accuracy of the estimates. Five parameters describing the individual contribution of three biological N_2O pathways were estimated accurately (variance/mean < 10% for all estimated parameters).

The NDHA model response was evaluated with statistical metrics (F-test, autocorrelation function). The 95% confidence intervals of DO and N_2O predictions based on the uncertainty obtained during calibration are studied for the first time. The measured data fall within the 95% confidence interval of the predictions, indicating a good model description. Overall, accurate parameter estimation and identifiability analysis of ammonium removal significantly decreases the uncertainty propagated to N_2O production, which is expected to benefit N_2O model discrimination studies and reliable full scale applications.

Keywords: Nitrous oxide, Respirometry, Uncertainty, Modelling, Parameter Estimation

1. Introduction

Nitrous oxide (N_2O) is a greenhouse gas emitted during biological nitrogen removal (BNR). The carbon footprint of wastewater treatment plants (WWTPs) is highly sensitive to N_2O emissions (Gustavsson and Tumlin, 2013), thus reducing N_2O emissions is beneficial for the energy balance of WWTPs.

During BNR operations biological and abiotic pathways are responsible of N_2O emissions (Schreiber et al., 2012). Ammonia-oxidizing bacteria (AOB) produce N_2O during incomplete ammonium (NH_4^+) oxidation to nitrite (NO_2^-) (nitrifier nitrification, NN). Under low dissolved oxygen (DO) AOBs use NO_2^- as the terminal electron acceptor and also release N_2O (nitrifier denitrification, ND). Heterotrophic denitrification is a 4-step process where N_2O is an obligate intermediate. Under low carbon-to-nitrogen ratios or in the presence of DO heterotrophic denitrification is not complete and N_2O can be released (HD) (Richardson et al., 2009). Hydroxylamine (NH_2OH) and free nitrous acid (HNO_2) are intermediates of NH_4^+ oxidation which can produce N_2O abiotically.

Process models are useful tools that translate our understanding of N_2O production into mathematical equations. N_2O model structures vary depending on the number of pathways, nitrogenous variables or parameters considered (Ding et al., 2016; Ni et al., 2014; Pocquet et al., 2016). The description of the autotrophic contribution transitioned form single- (NN or ND) to two-pathway (NN and ND) models to capture the N_2O dynamics observed during N-removal (Pocquet et al., 2016; Schreiber et al., 2009). Recently, a consilient N_2O model was proposed (NDHA, Nitrifier nitrification, nitrifier Denitrification, Hetrotrophic denitrification and Abiotic) that predict three biological pathways and abiotic processes (Domingo-Félez and Smets, 2016). Potentially, the NDHA model describes N_2O production under a wide range of operational conditions.

N_2O models are extensions of existing structures describing nitrogen removal and thus, calibration of N_2O dynamics also requires accurate predictions of the primary substrates (i.e.

DO, NH_4^+, NO_2^- , etc.). The experimental datasets used for calibration in lab-scale systems are either directly obtained from the reactor performance (Ding et al., 2016) or by conducting batch experiments (Ni et al., 2011). Initially, the information content of the experimental design was not studied because models aimed at describing N_2O trends without focusing on rigorous calibrations (Law et al., 2011). However, the amount and quality of data of the experimental design directly impact the calibration results (Dochain and Vanrolleghem, 2001).

Some studies report the proposed calibration framework (Guo and Vanrolleghem, 2014), but the N_2O parameter estimation procedures are often ill-described, with little information about each step. For example, the parameter subset selection considered during parameter estimation is sometimes not addressed. Local sensitivity measures are used as rankings for parameter selection (Pocquet et al., 2016; Spérandio et al., 2016), but these rankings are dependent on the initial parameter values and do not capture parameter interactions (Brun et al., 2001).

The overall fit and capabilities to describe N_2O dynamics has relied on analysis from best-fit simulations (e.g. R^2), which can lead to ambiguous results that cannot discriminate between models (Lang et al., 2017; Pan et al., 2015). A more rigorous analysis of residuals (e.g. Gaussian distributions, autocorrelation functions (ACF), F-test, etc.) would benefit the validation of the model response (Bennett et al., 2013).

Also, addressing the practical identifiability of newly estimated parameters will improve N_2O model discriminations procedures. For example, the parameter variance and correlation matrix are indicators of the confidence that can be given to a value, but they are not always reported, which makes it difficult to compare between N_2O model predictions (Ding et al., 2016; Kim et al., 2017; Pocquet et al., 2016; Spérandio et al., 2016). Practical identifiability problems might contribute to the large variability of parameter values in N_2O models (Domingo-Félez et al., 2017).

The uncertainty obtained during calibration translates into confidence intervals for model predictions. The accuracy, or width of the confidence interval, associated to the N_2O emissions

will be a key factor to consider during the development of mitigation strategies. Yet, the uncertainty of N_2O emissions associated to model calibration is not studied.

The objective of this study is to demonstrate and evaluate a standardized procedure for parameter estimation from N_2O models that relies on respirometric assays and in particular its application to analyse and validate the recently developed NDHA models. These assays are designed to allow the sequential fit of model components. The novelty resides in improving N_2O calibration procedures by targeting sources of uncertainty. Subsequently, the calibration results and associated uncertainty are evaluated. The calibration approach presented is a rigorous tool beneficial for N_2O model discrimination.

2. Material and Methods

2.1. Experimental Design

Nitrifying enrichment culture.

A lab-scale nitrifying sequencing batch reactor (5 L) was operated and displayed stable performance for three months after enrichment from an AS mixed liquor sample. Synthetic wastewater (modified after Graaf et al., 1996) with NH_4^+ as the only nutrient was fed at 0.5 g NH_4^+-N/L·d and a constant aeration rate maintained oxygen-limited conditions (DO below 0.25 mg/L) (SI-S1). NH_4^+ removal was 82 ± 14%, and nitritation efficiency ($NO_2^-/NH_4^+{}_{removed}$) at 85 ± 24% (Su et al., 2017). The biomass composition, based on 16 rRNA targeted qPCR analysis had a dominance of AOB over NOB (30:1) and agreed with the calculated based on the reactor performance (23:1). Detailed information of the qPCR analysis can be found in (Terada et al., 2010).

Monitoring nitrification and N_2O production via extant respirometric assays.

Biomass samples were harvested towards the end of the react cycle by centrifugation at 3600 g for 5 min, washed and resuspended in nitrogen-free mineral medium three times to eliminate any soluble substrate.

Assays were performed in parallel at 25°C in two 400-mL jacketed glass vessels completely filled with biomass and sealed with the insertion of a Clark-type polarographic DO electrode (YSI Model 5331, Yellow Springs, OH). Biomass samples were saturated with air or pure oxygen prior to the initiation of the respirometric assays. A decrease in the DO level in the vessel due to substrate oxidation was measured by the DO probe and continuously acquired by a personal computer interfaced to a DO monitor (YSI Model 5300, Yellow Springs, OH) by a multi-channel data acquisition device (LabPC+, National Instruments, Austin, TX). DO profiles were acquired at a user-defined frequency below the response time of the sensor (0.2 Hz). Liquid N_2O concentrations were measured with Clark-type microsensors (N2O-R, Unisense

A/S, Aarhus, Denmark) and pH (WTW GmbH, Weilheim, Germany). Stock solutions for all the reagents were prepared from high-purity chemicals for NH_4HCO_3, $NH_2OH \cdot HCl$, $NaNO_2$, $C_3H_5NaO_2$ (Sigma Aldrich) and by sparging ≥99.998% gas in deionized water for N_2O (Sigma-Aldrich). Photometric test kits were used to analyze N-substrates (1.14752, 1.09713, 1.14776, Merck KGaA, Darmstadt, Germany).

[Table 1]

Experimental Design

The aim of the experimental design was to obtain informative data on N_2O dynamics for a nitrifier dominated biomass to allow estimation of parameters of the NDHA model, which captures processes associated with nitrification, denitrification, and abiotic processes. Respirometric approaches were exclusively taken (on-line, high-rate O_2 and N_2O measurements) as they allow accurate parameter estimates compared to substrate depletion experiments (Chandran et al., 2008). The kinetics of the oxidation of the primary N-substrates (NH_4^+, NH_2OH and NO_2^-) were individually and step-wise, measured via extant respirometry under various initial DO conditions, with continuous N_2O measurements (Table 1). Then the interaction between the different N species was ascertained by liquid sampling at the end of certain experiments. In addition, specific experiments were conducted to measure the heterotrophic and abiotic contributions to total N_2O production during nitrification. Biomass content (MLSS, MLVSS) was measured in duplicates according to APHA (APHA et al., 1999).

The purpose was to predict the fate of the primary N-substrates based on the specific oxygen-consuming rate. By sequentially adding substrate pulses from oxidized to reduced form ($NO_2^- \rightarrow NH_2OH \rightarrow NH_4^+$), the individual rates can be isolated (Brouwer et al., 1998). The N_2O dynamics from NH_4^+ removal at varying NO_2^- and DO concentrations can be investigated simultaneously.

Scenarios (Batches grouped by substrate added: NH_4^+, NH_2OH, NO_2^-)

A scenario (e.g. Scen_AMO) was defined as a group of experiments with the same primary N-substrate added by pulses (Table 1). The overall oxygen consumption was the additive effect of several independent oxygen consumption processes, potentially including endogenous -, NO_2^- -. NH_2OH -, and NH_4^+-oxidation processes.

2.2. N_2O model description: NDHA

The NDHA model was proposed as a consilient model to describe N_2O dynamics under a variety of conditions for biomass containing both autotrophic and heterotrophic fractions (Domingo-Félez and Smets, 2016). It considers N_2O production from two autotrophic and one heterotrophic biological pathways, plus abiotic N_2O formation based on recent findings (Soler-Jofra et al., 2016). Unlike any other model, NDHA can qualitatively capture NO and N_2O profiles that have observed at high and low DO (Castro-Barros et al., 2016; Kampschreur et al., 2008; Rodriguez-Caballero and Pijuan, 2013; Yu et al., 2010). Here we aim to calibrate the NDHA model.

The following summarizes the essential and unique components of NDHA; for more information see (Domingo-Félez and Smets, 2016). The two autotrophic pathways have two different NO-producing processes, which are combined into a single N_2O-producing process. In Nitrifier Nitrification (NN), NO_{NN} is produced during NH_4^+ oxidation (AOR) under oxic conditions. Higher AOR will likely increase NO_{NN} and also N_2O. A fraction of NH_4^+, proportional to AOR is always released as N_2O_{NN}. In autotrophic denitrification (ND), under low DO NO_{ND} is produced by the reduction of HNO_2 with NH_2OH. This step is negatively affected by DO. The reduction of both NO_{ND} and NO_{NN} is lumped in one process with no oxygen inhibition as it is not known whether both NIR and NOR steps are directly inhibited by DO (Kozlowski et al., 2014). Thus, if NIR is inhibited by DO the overall ND-associated N_2O production will be indirectly limited. The 4-step denitrification model was considered based on (Hiatt and Grady, 2008). Individual process rates and inhibition/substrate coefficients were used as suggested for systems with low substrate accumulation. Nitrification produces HNO_2 and

182 NH_2OH. Abiotically NH_2OH can form HNO which dimerizes via $H_2N_2O_2$ to N_2O and H_2O (Eq.
183 i). HNO accumulation could occur due to an imbalance between the two reactions, leading to
184 chemical N_2O production (Igarashi et al., 1997). Nitrosation of NH_2OH (Eq. ii) has also been
185 postulated as a relevant reaction in partial nitrification reactors (Soler-Jofra et al., 2016).

186 $$NH_2OH \rightarrow HNO \rightarrow H_2N_2O_2 \rightarrow N_2O + H_2O \qquad \text{(Eq. i)}$$

187 $$NH_2OH + HNO_2 \rightarrow N_2O + H_2O \qquad \text{(Eq. ii)}$$

188 The pH data was used as input to the model to calculate the corresponding NH_3 and HNO_2
189 concentrations.

190 ### 2.3. Parameter estimation procedure

191 The steps in the parameter estimation procedure were to (1) estimate the best fit parameters to
192 describe O_2 consumption and N_2O production during the various (or during each type of)
193 experimental scenarios (Figure 1), (2) estimate the contribution of separate pathways to the total
194 N_2O production, and (3) quantify the uncertainty of model predictions.

195 [Figure 1]

196 #### 2.3.1. Parameter subset selection - Global sensitivity analysis

197 A global sensitivity analysis (GSA) was performed to identify the parameters most determinant
198 of model outputs by linear regression of Monte-Carlo simulations (Sin et al., 2009). Uncertainty
199 from model parameters was propagated as 10-25-50% uniform variations from their default
200 value to model outputs. Latin hypercube sampling was used to cover the parameter space. The
201 Standardized Regression Coefficient method was used to calculate the sensitivity measure β_i,
202 which indicates the effect of the parameter on the corresponding model output (Campolongo
203 and Saltelli, 1997) (convergence found with 500 samples). The duration of every experiment
204 was discretized in 400 parts and the GSA run at each point (SI-S2).

205 Parameters describing the elemental biomass composition (e.g. i_{NXB}), yield and temperature
206 coefficients were fixed at default values and not considered for calibration. For each scenario

the top ranked most sensitive parameters were preliminary selected as candidates for parameter estimation. All possible combinations of parameter candidates were assessed by increasing the size of the calibration subset to find the largest identifiable subset with the lowest error, assessed by the Akaike Information Criterion (AIC) (Akaike, 1974). To compare the information content of different parameter subsets of the same size the optimal experimental design criteria modE (Dochain and Vanrolleghem, 2001) was calculated together with RDE (Ratio of normalized D to modified E criteria), which captures the accuracy and precision of a calibrated subset (Machado et al., 2009). Newly estimated parameters were fixed at their best-fit estimate on the next calibration step (Figure 1).

2.3.2. Error minimization

The error function for problem minimization was defined as:

$$\text{Error} = \sum_{j}^{m} \frac{1}{n} \sum_{i}^{n} \left(\frac{y_{sim,i} - y_{obs,i}}{\sigma_i} \right)^2$$

Where m is the number of experiments in one scenario (e.g. 2 NOB experiments in Scen_NOB), n the number of experimental points of each experiment, $y_{sim,i}$ the model prediction and $y_{obs,i}$ the experimental data at time i, and σ_i the standard error of the experimental data. The minimization problem was started with global search method over a wide parameter space (GlobalSearch algorithm). From the estimated minimum, multiple local searches (PatternSearch algorithm) were started randomly in a narrower parameter space to avoid local minima. Model simulations were performed in the Matlab environment (The Mathworks Inc., Natick, USA).

2.3.3. Validation of model response and parameter estimates

To test the validity of the model response (i.e. the adequacy of model to predict the observed data points) the residuals ($y_{sim,i}$ - $y_{obs,i}$) were compared to a Gaussian distribution with a one-sample Kolmogorov-Smirnov test (Lilliefors, 1967). Interdependency of residuals was analysed by autocorrelation for different lag times (Cierkens et al., 2012). The quality of the model fit was calculated via correlation coefficients (R^2) and challenging the hypothesis of the linear

regression with simultaneous unit slope and zero intercept, where a value of 0/1 indicates a bad/good model fit (F-test). Moreover, by separating the error into three components: means, slope differences and randomness the Mean Squared Error Prediction (MSEP) index identifies the main error source between randomness, mean and standard deviation of residuals (NC, ME, SE) (Haefner, 2005). The prediction accuracy and the validation of the model to individual experiments was evaluated by the Root Mean Squared Error (RMSE) and the Janus coefficient to compare the RMSE between model calibration and validation (Power, 1993).

Based on the Fisher Information Matrix (FIM) collinearity indices were calculated to evaluate the identifiability of parameter estimates (Brun et al., 2001). Approximate confidence regions were calculated following $\mathrm{J_{crit}} = \mathrm{J_{opt}}\left(1 + \frac{p}{N_{data}-p} F_{\alpha,p,N_{data}-p}\right)$ (Beale, 1960). Coefficients of variation (CV) were described as the ration between the variance (σ) and the mean (μ) of the estimate.

The reliability of predictive distributions (95% confidence intervals) was evaluated by calculating the Percentage of observations within the Unit Confidence Interval (PUCI) (Li et al., 2011), which combines the fraction of experimental points inside the confidence interval (PCI) and the Average Relative Interval Length (ARIL) $\mathrm{ARIL_{0.95}} = \overline{\left(\mathrm{Limit_{Upper,0.95}} - \mathrm{Limit_{Lower,0.95}}\right)}/\mathrm{Data}$ (Jin et al., 2010). A smaller ARIL value (narrow distance between upper and lower 95% CI predictions) and a larger PUCI represent a better performance.

2.4. Uncertainty evaluation

The effect of directly estimated versus assumed parameter uncertainty was evaluated by Monte-Carlo simulations. The parameter distribution was sampled via LHS (n = 500) for two cases: from the distributions obtained during calibration, and compared to uncertainty classes assumed from literature as a reference case (Sin et al., 2009). The resolution of prediction uncertainty was assessed by the ARIL.

3. Results

3.1. Oxygen consumption during respirometric assays.

Each scenario grouped experiments based on the substrate added: NO_2^- (Scen_NOB) NH_2OH (Scen_HAO) or NH_4^+ (Scen_AMO). In all scenarios, even prior to any substrate spikes, oxygen consumption was always positive and proportional to the biomass concentration due to endogenous respiration. After substrate addition, oxygen consumption increased, to a much higher rate with NH_4^+ or NH_2OH than with NO_2^- spikes (Figure 2). The lower NO_2^- oxidizing rate of the biomass agreed with the measured low NOB vs AOB abundance (ca. 1:30). pH was not controlled and varied between 7 and 8, decreasing during NH_4^+ oxidation and increasing during reaeration periods due to CO_2 stripping or by manual base addition (NaOH).

[Figure 2]

The ranking from the averaged GSA for DO shows that the sequential scenarios (measuring the respirometric response to addition of synthetic substrates) provides sufficient information to individually estimate the relevant biokinetic parameters of each step in the ammonium oxidation process (Figure 3). For example, in Scen_NOB the maximum growth rate for NOB (μ_{NOB}) ranked first, while in Scen_AMO the substrate affinity ($K_{AOB.NH3}$) and maximum growth rate for the AMO ($\mu_{AOB.AMO}$) step ranked in the top.

[Figure 3]

3.1.1. Estimation of primary substrate kinetics based on DO profiles

Initial conditions for each batch were defined by simulating endogenous decay and hydrolysis with default parameters. The objective of the parameter subset selection was to calibrate the minimum number of identifiable parameters that explain the data. A total of five parameters could be estimated from the aerobic scenarios (Table 2). The calibrated parameters for Scen_NOB were μ_{NOB} and k_H, for Scen_AMO μ_{AMO} and $K_{AOB.NH3}$, and for Scen_AMO_DO $K_{AOB.O2.AMO}$ (Table 2). To illustrate the procedure used for every scenario results from

Scen_NOB and Scen_AMO are summarized in the SI (SI-S3). The electron distribution in AOB differs between NH_4^+ (Scen_AMO) oxidation and isolated NH_2OH oxidation (Scen_HAO) (SI–S4). Hence, parameter estimation results from Scen_HAO were not considered representative of NH_4^+ oxidation, our targeted process. To describe more accurately the low NH_2OH concentration values reported in literature (Soler-Jofra et al., 2016) the affinity for NH_2OH, $K_{AOB.NH2OH}$, was increased compared to other N_2O models (SI–S4). The oxygen consumption rate of NH_4^+ experiments drops quickly to endogenous levels (Figure 2, C). The lack of an intermediate oxygen uptake rate indicates that no significant accumulation of an intermediate which agrees with the proposed higher affinity for NH_2OH (2.29 mgCOD/mgN). [Table 2]

Validation of model response (DO) and primary N-substrate parameter estimates

The model consistently described the experimental DO profiles for every scenario (F-test = 1, which indicates that we fail to reject the null hypothesis of slope 1 and intercept 0 between simulations and observations) (Figure 4, A, B). The MSEP indicated that randomness was the main source of error compared to the mean or standard deviation, validating the model response during calibration (NC > ME, SE, SI-S5). The uncertainty of the parameter estimates (Table 2) was propagated to the model predictions, showing an increased resolution of the 95% predictive distributions for DO compared to the uncertainty of the reference case (ARIL = 3.8/0.5 before/after parameter estimation). The PUCI (percentage of observations bracketed by the unit confidence interval) also improved from 0.4 to 1.5.

Best-fit parameter estimates at each scenario were estimated at high accuracy: coefficients of variation (CV) were below 7% for all cases (Table 2) and the collinearity indices below 15, as suggested for identifiable subsets (Brun et al., 2002) (SI-S3). The high correlation between $\mu_{AOB.AMO}$-$K_{AOB.NH3}$ typically occurs for Monod-type kinetics but it did not affect their identifiability.

While the error distribution of each scenario was not normally distributed (Kolmogorov-Smirnov test 95%), no systematic deviations were observed (Figure 4). The analysis of the

residuals indicated that for scenarios AMO and NOB the errors were autocorrelated (SI-S5). Subsequently, the effect of sampling resolution on the optimal parameter values and uncertainties was minimized until the autocorrelation obtained was negligible (SI-S5). As the sampling data frequency decreased through subsampling, the accuracy of estimates decreased too (e.g. $CV\mu_{AOB.AMO}$ = 2% point/2 min, 4.4% point/10min). However, the lower precision of the best-fit estimates did not translate into higher simulation uncertainty for the primary N-substrates ($\sigma_{95\%CI}$ increased by less than 0.06 mg/L for DO, NH_4^+, NH_2OH or NO_2^-). Consequently, while the autocorrelation of residuals affected the DO parameter estimation results it did not impact the N_2O calibration, the focus of this study.

[Figure 4]

The fitted model was evaluated on five additional experiments not used during calibration with varying initial pH (7-8), NO_2^- (0-6.2mgN/L) and NH_4^+ pulses (1-10mgN/L). The Janus coefficient and R^2 were close to unity (1.24 and 0.997) indicating a good model validation (Figure 4, C, D). In sum, the respirometric experimental design can be used to precisely identify and calibrate the primary substrate dynamics of the NDHA model based on the DO profiles.

3.2. Dynamics of N_2O during different scenarios

In the same scenarios considered for DO calibration liquid N_2O was also continuously measured (Figure 2). Moreover, the role of the primary N-substrates (NH_4^+, NH_2OH, NO_2^-, and NO_3^-) on N_2O production was also studied under anoxic conditions (Table 1). Under conditions heterotrophic denitrification (Scen_An_HB) the presence of NO_2^- and NO_3^- did not show any net N_2O production (data not shown). However, N_2O was consumed after sCOD addition when no other N-substrate was present, indicating a positive HD contribution to the total N_2O pool (Figure 5). During NO_2^- oxidation experiments or at the onset of anoxia in the presence of NO_2^- and NO_3^- no N_2O production was detected (Figure 2, A).

AOB-driven NH_4^+ oxidation (Scen_AMO) produced a small amount of N_2O under aerobic conditions and significantly increased at the onset of anoxia (Figure 2). The specific N_2O production rate (mgN_2O-N/gVSS.min) obtained in duplicate experiments – carried out at varying biomass concentrations – were in close agreement, thus indicating biologically-driven N_2O production (SI-S6).

The role of NH_2OH as a direct precursor of N_2O was investigated in Scen_HAO. Under aerobic conditions, NH_2OH oxidation produced more N_2O than NH_4^+ oxidation. In addition, upon reaching anoxia the N_2O production rate also increased in the presence of NH_2OH (Figure 2, B). Under anoxic conditions (Scen_An_AOB) neither NH_4^+ nor NO_2^- produced N_2O individually (SI-S6). The spike of NH_2OH yielded the largest amount of N_2O specific to the amount of nitrogen spiked, and NO_2^- was not detected at the end of the experiment (NO_2^- < 0.05 mgN/L). Hence, NH_2OH oxidation by AOB produces N_2O and does not require O_2. The addition of an electron acceptor like NO_2^- to ongoing anoxic NH_2OH oxidation increased the net N_2O production rate, while addition of an electron donor as NH_4^+ did not (SI-S6).

Taken together, the N_2O production observed in all the scenarios can only be effectively predicted using the NDHA model compared to other N_2O models, especially the DO-independent N_2O production from NH_2OH oxidation and no NO_2^- production (Ding et al., 2016; Domingo-Félez and Smets, 2016; Ni et al., 2014; Pocquet et al., 2016).

3.2.1. Parameter estimation from N_2O dynamics

In the absence of stripping, heterotrophic denitrification is the only N_2O consuming process. First, the N_2O consumption potential of the biomass was estimated and the reduction factor was considered representative for the 4-step heterotrophic denitrification processes (η_{HD} = 0.055) (Figure 5, A). Then, N_2O production observed from NH_4^+ oxidation at high DO, where the interference of the two denitrifying pathways is minimum, was used to calibrate the NN pathway. ε_{AOB}, the most sensitive parameter at high DO was calibrated, ε_{AOB} = 0.00048 (Figure 5, B, SI-S2). Experiments from Scen_AMO were designed to reach anoxia at varying HNO_2

concentrations (0.15-3 μgN/L). Parameters associated to the ND pathway were the most sensitive and were thus calibrated (η_{NOR} = 0.16, $K_{AOB.HNO2}$ = 0.67 μgN/L, $K_{NH2OH.ND}$ = 0.25 mgN/L) (SI-S2, S7). The abiotic contribution measured was low and not considered during in the final Gujer matrix (SI-S10). A total of five parameters could be estimated from the N_2O datasets of all the scenarios (Table 2).

[Figure 5]

Validation of model response and secondary substrate (N_2O) parameter estimates

The calibrated NDHA model described the N_2O production dynamics and yield observed in the calibration datasets (F-test = 1). In all but one of the assays randomness was the most important part of the error based on the MSEP analysis (SI-S5). After calibration the ARIL narrowed by 58% from the original resolution and the PUCI increased by 71% (n = 6 assays).

The predictive ability of the model was evaluated on three batches with lower HNO_2 and with higher NH_2OH pulses (HNO_2 < 0.15 μgN/L, NH_2OH = 2 mgN/L). The average Janus coefficient of the validation prediction was 1.57 and R^2 was 0.985, indicating a good validation (Figure 5, D, E, F). Hence, the NDHA model could describe the N_2O production rates at a range of DO and HNO_2 concentrations.

The simple experimental design allowed the isolation of the various components of N_2O dynamics during NH_4^+ oxidation, and the parameter estimation procedure the identification of relevant model parameters.

3.3. Model predictions under varying DO and HNO_2: Scenario analysis

To investigate the effect of DO and HNO_2 on N_2O production the NDHA model was evaluated at varying DO and HNO_2 concentrations at pH = 7.5 (Figure 6) with the newly estimated parameters. The model predicted the largest N_2O emission at the lowest DO and high HNO_2 (> 20%, SI-S8); and the lowest N_2O emission at the highest DO and lowest HNO_2 (0.13%). The effect of increasing HNO_2 is seen at every DO level ($DO_{0.3}$: 0.33 → 5.4%, $DO_{5.0}$: 0.13 →

382 0.28%). Conversely, increasing DO lowered the N_2O emission factor regardless of the HNO_2
383 level. The NO emission showed an increasing pattern with HNO_2 but a minimum was found at
384 DO = 2.0 mg/L, further increasing at higher DO (SI-S8).

385 The contribution of the NN pathway was maximum when HNO_2 was not present and decreased
386 with increasing HNO_2, at a faster rate at lower than at higher DO (2.4 and 47% respectively).
387 The ND contribution followed opposite trends, indicating a shift between autotrophic pathways
388 driven by HNO_2 and DO. The ND contribution increased with HNO_2, at a steeper rate at lower
389 DO (97.4%) than at higher (53%). The HD contribution was maximum at low DO and high
390 HNO_2 but only reached 0.2% (SI-S8).

391 [Figure 6]

392

393 ## 4. Discussion

394 ### 4.1. Parameter estimation from respirometric assays: oxygen consumption

395 The respirometric experiments were used to investigate the oxygen-consuming processes driven
396 by the AOB-enriched biomass in the presence of reduced N-species (NH_4^+, NH_2OH and NO_2^-).
397 If a model captures accurately the relevant oxygen-consuming processes, then DO and the
398 primary N-substrates are predicted accurately. The experimental design based on the
399 concatenated oxygen consumption allowed the isolation of individual processes independently
400 (endogenous → NO_2^- → NH_4^+) (Chandran and Smets, 2005).

401 The calibrated model could describe the endogenous oxygen uptake and NO_2^- oxidation in
402 Scen_NOB. However, because of the low NOB abundance the oxygen consumption from NO_2^-
403 oxidation was low, shown by a similar sensitivity of NOB and endogenous parameters to
404 oxygen consumption after NO_2^- spikes (Figure 3).

405 In Scen_AMO oxygen consumption was very sensitive to NH_4^+ dynamics (SI-S2), which
406 yielded precise estimates for $\mu_{AOB.AMO}$, $K_{AOB.NH3}$ and $K_{AOB.O2.AMO}$ (Table 2). The maximum AOB
407 growth rate ($\mu_{AOB.AMO}$ = 0.49 1/d) is in the low range of literature values found for N. *europaea*
408 (0.56-1.62 1/d) (Brockmann et al., 2008). The biomass concentration (X_{AOB}), growth yield
409 (Y_{AOB}) and maximum growth rate cannot be simultaneously identified from short experiments
410 solely with DO data (Ellis et al., 1996; Petersen et al., 2001). Hence, the estimated growth rate
411 is linearly dependent on the fixed values for X_{AOB} and Y_{AOB}: a lower initial condition for X_{AOB}
412 would yield a higher estimate for $\mu_{AOB.AMO}$. Overall, the maximum specific NH_4^+ oxidation,
413 7.54±0.1E-05 $gN/gVSS_{(AOB)}/h$, was similar to other literature values for an AOB-enriched
414 biomass (Ciudad et al., 2006). For the same NH_4^+ concentration, the higher oxygen consumption
415 rate observed at higher pH was predicted by considering NH_3 the true substrate. The estimated
416 affinities for both NH_4^+ oxidation substrates ($K_{AOB.NH3}$ = 0.12 mgN/L, $K_{AOB.O2.AMO}$ = 0.23 mg/L)
417 were in range of literature values (Magrí et al., 2007; Park and Noguera, 2007).

418 Overall, the precision of the identified parameter was high (CV < 7%), common from
419 respirometric studies (Petersen et al., 2001). It should be noted that the concentration of the

spikes did not include uncertainty and was not estimated, which decreased the uncertainty of model predictions (Gernaey et al., 2002).

4.2. Role of NH_4^+ oxidation intermediates on N_2O production: experimental and modelling results

Nitrification plays an important role on N_2O emissions from N-removing systems, where NH_4^+, NO_2^- and DO are the main substrates. Experimental results indicated that aerobic NH_4^+-oxidation products, NH_2OH and NO_2^- were responsible for the higher N_2O production rate at the onset of anoxia and not NH_4^+ itself, which requires molecular O_2 for its oxidation (Sayavedra-Soto et al., 1996) (SI-S6). NH_2OH has been shown to be a key compound regulating N_2O production by AOB (Caranto et al., 2016; de Bruijn et al., 1995; Kozlowski et al., 2016). Because of its high reactivity under aerobic and anoxic conditions, it is an important electron donor for the cytochrome pool of AOB. Previous studies have shown the higher N_2O yield of nitrifying biomass and pure cultures fed on NH_2OH compared to NH_4^+, also observed in Scen_HAO ($N_2O\_R_{NH2OH}/N_2O\_R_{NH4+}$ = 40) (Figure 2) (Kim et al., 2010; Kozlowski et al., 2016). Here we show that even under anoxic conditions the sole presence of NH_2OH also yields a large amount of N_2O (SI-S6), suggested as a new N_2O producing pathway by (cyt) P460 (Caranto et al., 2016). The addition of an electron donor like NO_2^- further increased N_2O production, highlighting the role of the primary N-substrates on N_2O dynamics, especially of NH_2OH.

The NDHA model captures the observed anoxic NH_2OH oxidation to N_2O with no HNO_2 production associated. A NH_2OH pulse in the concentration range of reported measurements (0.1mgN/L) could be described in the calibration dataset (Figure 5, F-test = 1, $R^2 > 0.99$); and at higher NH_2OH concentrations (2 mgN/L) the model predicted the N_2O trend but not as accurately (Figure 5, F-test = 0, $R^2 = 0.97$). Anoxic NH_2OH oxidation to NO has been recently proposed by Caranto and Lancaster (2017) as the HAO-catalyzed reaction, where NO_2^- is produced only under aerobic conditions. The NO and NO_2^- producing reactions, together with

446 the anoxic NO reduction to N_2O are captured by the NDHA model (SI-S10, Process 2, 3, 5).
447 Based on the model structure of other two-pathway models for AOB none can predict the
448 observed N_2O dynamics. In certain models NH_2OH does not react under anoxic conditions
449 (Ding et al., 2016; Pocquet et al., 2016), or reacts producing both N_2O and HNO_2 (Ni et al.,
450 2014).

451 Under a variety of DO, HNO_2 and NH_3 concentrations the calibrated NDHA model could
452 describe the observed N_2O dynamics. Other models, with varying degrees of complexity, have
453 also described the effect of HNO_2 and DO (4-6 processes) but the effect of NH_2OH, the main
454 driver of N_2O production, was not considered (Ding et al., 2016; Ni et al., 2014). The scenario
455 analysis indicated a shift between the main pathway contributions governed by DO and HNO_2
456 (Figure 6). This relationship has been described by other two-pathway models, where ND was
457 the main contributor to the N_2O emission factor during NH_4^+ oxidation and the highest N_2O
458 emission factor was observed at low DO (Ni et al., 2014; Pocquet et al., 2016).

459 **4.3. N_2O model calibration**

460 **4.3.1. Analysis of the NDHA parameter estimates.**

461 In the last years new N_2O models have improved their best-fit predictions under different
462 scenarios (i.e. varying DO, NO_2^-) by increasing the number of processes and variables
463 considered. For example, all the models describe the ND pathway with a NO_2^- dependency (Ni
464 et al., 2011; Pocquet et al., 2016; Schreiber et al., 2009), or the NN pathway as a fraction of the
465 NH_2OH oxidation to NO_2^- (Ni et al., 2014; Pocquet et al., 2016). While the intermediates of
466 NH_4^+ oxidation or the process rates are described differently, some parameters are common
467 across N_2O models.

468 In this study, the contribution of the NN pathway (ε_{AOB} = 0.048% $\mu_{AOB.HAO}$) is in the low range
469 of other reported values (0.052-0.15%), while the maximum N_2O production rate, described by
470 η_{NOR} = 0.16, lies in the range (0.07 – 0.34). In agreement with the ND description of the model
471 by Pocquet et al., (2016), the electron acceptor of the ND pathway was HNO_2 instead of NO_2^-.

Increasing N_2O production rates were observed at higher HNO_2 but constant NO_2^- (9.5-10mgN/L, 0.8-1.5 μgHNO_2-N/L). The affinity for HNO_2 ($K_{AOB.HNO2}$ = 0.67 μgHNO_2-N/L, 17.1 mg NO_2^--N/L, pH 7.5, 20 ºC) could be estimated from experiments run at varying HNO_2 (0.16-1.5 μgHNO_2-N/L). The affinity for NO_2^- is 100 times lower than other nitrifying systems, but 15 times higher than a NO_2^--accumulating biomass ($K_{AOB.NO2-}$ = 0.14, 282 mgN/L)(Pocquet et al., 2016; Schreiber et al., 2009). The difference could be explained by the operating conditions at which each biomass is acclimated: low NO_2^- for activated sludge systems (≈ 0.5mgN/L) and high NO_2^- for nitritating reactors (50-150 mg NO_2^--N/L in the parent reactor of this study). The NDHA model combined with the experimental design allows the simultaneous estimation of parameters describing main N-substrates and N_2O dynamics from simple respirometric experiments.

4.3.2. N_2O models: response validation and identifiability

As N_2O models produce better fits discrimination tools become more important. If the capabilities of two models to describe dynamic N_2O trends are similar (Lang et al., 2017; Pan et al., 2015) visual inspection or metrics such as R^2 are not sufficient, and more rigorous statistics as the F-test used in this study are necessary for model discrimination.

The parameter subset selection during calibration of each scenario was based on the lower AIC criteria. The identifiability of the estimated parameters was assessed by the correlation matrix and the precision of the estimated parameters (CV < 5%). The triplet $K_{AOB.HNO2}$, $K_{AOB.NH2OH.ND}$ and η_{NOR} were estimated with the same dataset, and based on their collinearity index ($\gamma > 15$) they are not identifiable and their values depend on the others. This metric is based on local sensitivities, and as shown in (Table 2), the high correlation between $K_{AOB.NH2OH.ND}$ and η_{NOR} could be responsible for the high collinearity of the triplet. An improved experimental design or an additional dataset such as NO would improve the identifiability these parameters, as shown for other two-pathway N_2O models (Pocquet et al., 2016). Together with the best-fit prediction

497 the 95% CI of the calibrated NDHA model bracketed the experimental datasets, validating the
498 model response.

499 The uncertainty of estimates (CV, correlation matrix) is not always reported in literature (Ding
500 et al., 2016; Kim et al., 2017; Spérandio et al., 2016), which hampers critical discrimination
501 procedures. While some models have reported the estimated variance identifiability metrics are
502 scarce and not assessed. To the authors knowledge none of the proposed N_2O models has
503 studied how the uncertainty of parameter estimates affects N_2O predictions (e.g. ARIL, PUCI).
504 Moreover, the analysis of residuals shows that high frequency data such as online sensors are
505 not totally discrete and can lead to autocorrelated residuals in N_2O measurements (SI-S5). When
506 residuals are not independent they are not randomly distributed. Practically this means
507 underestimation of the sample variance because each data point was presumed an independent
508 random observation. This then leads to underestimation of the parameter uncertainty (Reported
509 CV $\ll$ 0.001% (Peng et al., 2015)). In this study, sub-sampling of sensor data has been used to
510 reduce the auto-correlation between two consecutive data points.

511 Hence, while very high precision of estimates is possible, testing the model response can avoid
512 a possible over interpretation of the dataset. In this study we show that addressing parameter
513 identifiability after model calibration will benefit N_2O model discrimination studies.

514 ### 4.4. N_2O model uncertainty

515 With the final objective of designing N_2O mitigation strategies, the confidence of model
516 predictions is critical when quantifying N_2O emissions. As a by-product of NH_4^+ oxidation, the
517 uncertainty associated to NH_4^+ removal processes will propagate to N_2O predictions. The
518 respirometric experimental design allowed for accurate estimates and narrow 95% confidence
519 intervals for DO, NH_4^+ and other N-species, which was critical to reduce the predicted
520 uncertainty for N_2O (SI-S9). N_2O models have been calibrated by sequentially fitting the
521 primary N-substrates followed by the N_2O dynamics (Ni et al., 2014; Pocquet et al., 2016). The
522 effect of propagating the uncertainty from the calibration of primary N-substrates to N_2O was

not discussed. Consequently, the precision of the N_2O calibration could be overestimated. Here, the heterotrophic contribution was accounted for during the calibration and analysed by propagating the uncertainty to all the biological parameters.

[Figure 7]

To evaluate the performance of the parameter estimation results N_2O emissions from a simulated case study were examined via Monte-Carlo simulations (pH = 7.5, NH_4^+ = 70 mgN/L, DO = 0.3, 1.3 mg/L and NO_2^- = 0, 1, 5, 15, 100 mgN/L, 500 simulations). At pseudo-steady state the standard error of the Monte-Carlo simulations shows the propagated uncertainty. For the 10 parameters estimated in this study the normalized uncertainty associated to their default class (Sin et al., 2009) is approximately 40% of the N_2O emission factor (Figure 7). If the calibration results from this experimental design are considered instead (Table 2), the uncertainty decreases to 10% (Figure 7). The accuracy of different N_2O models calibrated with the same dataset could be also compared with this methodology. These results highlight the importance of considering uncertainty propagation in N_2O predictions, as N_2O emissions are greatly affected by the uncertainty of primary N-substrates.

Conclusions

- A novel experimental design to calibrate N_2O models through extant respirometry is proposed that combines DO and N_2O measurements.
- Parameters associated to NO_2^- and NH_4^+ oxidation were sequentially fitted to DO consumption profiles by isolating individual processes. Five parameters were identified from the DO dataset and another five were estimated from the N_2O dataset with low uncertainty (CV < 10%).
- The NDHA model response was validated and described AOB-driven N_2O production at varying DO and HNO_2 concentrations.
- For the first time the uncertainty of the calibrated parameters was propagated to the model outputs in a simulation case study, and compared to the uncertainty from a

549 reference case. The uncertainty of the N_2O emission factor predicted was reduced from
550 ~ 40% of its value to ~ 10%.

551 **Software availability**

552 The MATLAB/SIMULINK code containing the implementation of the model is free upon
553 request to the corresponding author.

554 **Acknowledgements**

555 This research was funded by the Danish Agency for Science, Technology and Innovation
556 through the Research Project LaGas (12-132633). Dr. Ulf Jeppsson (Lund University) is
557 acknowledged for having provided the codes of the Benchmark Simulation Model no 2 from
558 which this work was developed. The authors have no conflict of interest to declare.

559

References

Akaike, H., 1974. A new look at the statistical model identification. IEEE Trans. Automat. Contr. 19, 716–723. doi:10.1109/TAC.1974.1100705

Beale, E.M.L., 1960. Confidence Regions in Non-Linear Estimation. J. R. Stat. Soc. Ser. B-statistical Methodol. 22, 41–88. doi:10.2307/2983877

Bennett, N.D., Croke, B.F.W., Guariso, G., Guillaume, J.H.A., Hamilton, S.H., Jakeman, A.J., Marsili-Libelli, S., Newham, L.T.H., Norton, J.P., Perrin, C., Pierce, S.A., Robson, B., Seppelt, R., Voinov, A.A., Fath, B.D., Andreassian, V., 2013. Characterising performance of environmental models. Environ. Model. Softw. 40, 1–20. doi:10.1016/j.envsoft.2012.09.011

Brockmann, D., Rosenwinkel, K.-H., Morgenroth, E., 2008. Practical identifiability of biokinetic parameters of a model describing two-step nitrification in biofilms. Biotechnol. Bioeng. 101, 497–514. doi:10.1002/bit.21932

Brouwer, H., Klapwijk, A., Keesman, K.J., 1998. Identification of activated sludge and wastewater characteristics using respirometric batch-experiments. Water Res. 32, 1240–1254. doi:10.1016/S0043-1354(97)00334-5

Brun, R., Kühni, M., Siegrist, H., Gujer, W., Reichert, P., 2002. Practical identifiability of ASM2d parameters--systematic selection and tuning of parameter subsets. Water Res. 36, 4113–27.

Brun, R., Reichert, P., Kfinsch, H.R., 2001. Practical identifiability analysis of large environmental simulation models. Water Resour. Res. 37, 1015–1030.

Campolongo, F., Saltelli, A., 1997. Sensitivity analysis of an environmental model: an application of different analysis methods. Reliab. Eng. Syst. Saf. 57, 49–69. doi:10.1016/S0951-8320(97)00021-5

Caranto, J.D., Lancaster, K.M., 2017. Nitric oxide is an obligate bacterial nitrification intermediate produced by hydroxylamine oxidoreductase. Proc. Natl. Acad. Sci. 201704504. doi:10.1073/pnas.1704504114

Caranto, J.D., Vilbert, A.C., Lancaster, K.M., 2016. Nitrosomonas europaea cytochrome P460 is a direct link between nitrification and nitrous oxide emission. Proc. Natl. Acad. Sci. 113, 14704–14709. doi:10.1073/pnas.1611051113

Castro-Barros, C., Rodríguez-Caballero, A., Volcke, E.I.P., Pijuan, M., 2016. Effect of nitrite on the N2O and NO production on the nitrification of low-strength ammonium wastewater. Chem. Eng. J. 287, 269–276. doi:10.1016/j.cej.2015.10.121

Chandran, K., Hu, Z., Smets, B.F., 2008. A critical comparison of extant batch respirometric and substrate depletion assays for estimation of nitrification biokinetics. Biotechnol. Bioeng. 101, 62–72. doi:10.1002/bit.21871

Chandran, K., Smets, B.F., 2005. Optimizing experimental design to estimate ammonia and nitrite oxidation biokinetic parameters from batch respirograms. Water Res. 39, 4969–78. doi:10.1016/j.watres.2005.10.001

Cierkens, K., Plano, S., Benedetti, L., Weijers, S., de Jonge, J., Nopens, I., 2012. Impact of influent data frequency and model structure on the quality of WWTP model calibration and uncertainty. Water Sci. Technol. 65, 233–42. doi:10.2166/wst.2012.081

Ciudad, G., Werner, A., Bornhardt, C., Muñoz, C., Antileo, C., 2006. Differential kinetics of ammonia- and nitrite-oxidizing bacteria: A simple kinetic study based on oxygen affinity and proton release during nitrification. Process Biochem. 41, 1764–1772. doi:10.1016/j.procbio.2006.03.032

de Bruijn, P., van de Graaf, A.A., Jetten, M.S.M., Robertson, L.A., Kuenen, J.G., 1995. Growth of Nitrosomonas europaea on hydroxylamine. FEMS Microbiol. Lett. 125, 179–184.

608 Ding, X., Zhao, J., Hu, B., Chen, Y., Ge, G., Li, X., Wang, S., Gao, K., Tian, X., 2016.
609 Mathematical modeling of nitrous oxide production in an anaerobic/oxic/anoxic process.
610 Bioresour. Technol. 222, 39–48. doi:10.1016/j.biortech.2016.09.092

611 Dochain, D., Vanrolleghem, P.A., 2001. Dynamic Modelling and Estimation in Wastewater
612 Treatment Processes. IWA Publishing, London, UK.

613 Domingo-Félez, C., Pellicer-Nàcher, C., Petersen, M.S., Jensen, M.M., Plósz, B.G., Smets, B.F.,
614 2017. Heterotrophs are key contributors to nitrous oxide production in activated sludge
615 under low C-to-N ratios during nitrification-Batch experiments and modeling. Biotechnol.
616 Bioeng. 114, 132–140. doi:10.1002/bit.26062

617 Domingo-Félez, C., Smets, B.F., 2016. A consilience model to describe N 2 O production
618 during biological N removal. Environ. Sci. Water Res. Technol. 2, 923–930.
619 doi:10.1039/C6EW00179C

620 Ellis, T.G., Barbeau, D.S., Smets, B.F., Grady, C.P.L., 1996. Respirometric technique for
621 determination of extant kinetic parameters describing biodegradation. Water Environ. Res.
622 68, 917–926. doi:10.2175/106143096X127929

623 Gernaey, K., Petersen, B., Dochain, D., Vanrolleghem, P.A., 2002. Modeling aerobic carbon
624 source degradation processes using titrimetric data and combined respirometric-titrimetric
625 data: structural and practical identifiability. Biotechnol. Bioeng. 79, 754–67.
626 doi:10.1002/bit.10337

627 Graaf, A.A. Van De, Bruijn, P. De, Robertson, L.A., Jetten, M.S.M., Kuenen, J.G., 1996.
628 Autotrophic growth of anaerobic am monium-oxidizing microorganisms in a fluidized bed
629 reactor. Microbiology 142, 2187–2196.

630 Guo, L., Vanrolleghem, P. a., 2014. Calibration and validation of an activated sludge model for
631 greenhouse gases no. 1 (ASMG1): prediction of temperature-dependent N2O emission
632 dynamics. Bioprocess Biosyst. Eng. 37, 151–163. doi:10.1007/s00449-013-0978-3

633 Gustavsson, D.J.I., Tumlin, S., 2013. Carbon footprints of Scandinavian wastewater treatment
634 plants. Water Sci. Technol. 68, 887. doi:10.2166/wst.2013.318

635 Haefner, J.W., 2005. Modeling Biological Systems: Principles and Applications, Second. ed.
636 Springer.

637 Hiatt, W.C., Grady, C.P.L., 2008. An updated process model for carbon oxidation, nitrification,
638 and denitrification. Water Environ. Res. 80, 2145–2156. doi:10.2175/106143008X304776

639 Igarashi, N., Moriyama, H., Fujiwara, T., Fukumuri, Y., Tanaka, N., 1997. he 2.8 A structure of
640 hydroxylamine oxidoreductase from a nitrifying chemoautotrophic bacterium,
641 Nitrosomonas europaea. Nature 4, 276–284.

642 Jin, X., Xu, C.-Y., Zhang, Q., Singh, V.P., 2010. Parameter and modeling uncertainty simulated
643 by GLUE and a formal Bayesian method for a conceptual hydrological model. J. Hydrol.
644 383, 147–155. doi:10.1016/j.jhydrol.2009.12.028

645 Kampschreur, M.J., van der Star, W.R.L., Wielders, H.A., Mulder, J.W., Jetten, M.S.M., van
646 Loosdrecht, M.C.M., 2008. Dynamics of nitric oxide and nitrous oxide emission during
647 full-scale reject water treatment. Water Res. 42, 812–26. doi:10.1016/j.watres.2007.08.022

648 Kim, M., Wu, G., Yoo, C., 2017. Quantification of nitrous oxide (N2O) emissions and soluble
649 microbial product (SMP) production by a modified AOB-NOB-N2O-SMP model.
650 Bioresour. Technol. 227, 227–238. doi:10.1016/j.biortech.2016.11.127

651 Kim, S.-W., Miyahara, M., Fushinobu, S., Wakagi, T., Shoun, H., 2010. Nitrous oxide emission
652 from nitrifying activated sludge dependent on denitrification by ammonia-oxidizing
653 bacteria. Bioresour. Technol. 101, 3958–63. doi:10.1016/j.biortech.2010.01.030

654 Kozlowski, J.A., Kits, K.D., Stein, L.Y., 2016. Comparison of Nitrogen Oxide Metabolism
655 among Diverse Ammonia-Oxidizing Bacteria. Front. Microbiol. 7, 1–9.
656 doi:10.3389/fmicb.2016.01090

Kozlowski, J. a, Price, J., Stein, L.Y., 2014. Revision of N2O-Producing Pathways in the Ammonia-Oxidizing Bacterium Nitrosomonas europaea ATCC 19718. Appl. Environ. Microbiol. 80, 4930–4935. doi:10.1128/AEM.01061-14

Lang, L., Pocquet, M., Ni, B.-J., Yuan, Z., Spérandio, M., 2017. Comparison of different two-pathway models for describing the combined effect of DO and nitrite on the nitrous oxide production by ammonia-oxidizing bacteria. Water Sci. Technol. 75, 491–500. doi:10.2166/wst.2016.389

Law, Y., Lant, P., Yuan, Z., 2011. The effect of pH on N2O production under aerobic conditions in a partial nitritation system. Water Res. 45, 5934–44. doi:10.1016/j.watres.2011.08.055

Li, L., Xu, C.-Y., Xia, J., Engeland, K., Reggiani, P., 2011. Uncertainty estimates by Bayesian method with likelihood of AR (1) plus Normal model and AR (1) plus Multi-Normal model in different time-scales hydrological models. J. Hydrol. 406, 54–65. doi:10.1016/j.jhydrol.2011.05.052

Lilliefors, H.W., 1967. On the Kolmogorov-Smirnov Test for Normality with Mean and Variance Unknown. J. Am. Stat. Assoc. 62, 399. doi:10.2307/2283970

Machado, V.C., Tapia, G., Gabriel, D., Lafuente, J., Baeza, J.A., 2009. Systematic identifiability study based on the Fisher Information Matrix for reducing the number of parameters calibration of an activated sludge model. Environ. Model. Softw. 24, 1274–1284. doi:10.1016/j.envsoft.2009.05.001

Magrí, A., Corominas, L., López, H., Campos, E., Balaguer, M., Colprim, J., Flotats, X., 2007. A Model for the Simulation of the SHARON Process: pH as a Key Factor. Environ. Technol. 28, 255–265. doi:10.1080/09593332808618791

Ni, B.-J., Peng, L., Law, Y., Guo, J., Yuan, Z., 2014. Modeling of Nitrous Oxide Production by Autotrophic Ammonia-Oxidizing Bacteria with Multiple Production Pathways. Environ. Sci. Technol. 48, 3916–24. doi:10.1021/es405592h

Ni, B.-J., Ruscalleda, M., Pellicer-Nàcher, C., Smets, B.F., 2011. Modeling nitrous oxide production during biological nitrogen removal via nitrification and denitrification: extensions to the general ASM models. Environ. Sci. Technol. 45, 7768–76. doi:10.1021/es201489n

Pan, Y., Ni, B.-J., Lu, H., Chandran, K., Richardson, D., Yuan, Z., 2015. Evaluating two concepts for the modelling of intermediates accumulation during biological denitrification in wastewater treatment. Water Res. 71, 21–31. doi:10.1016/j.watres.2014.12.029

Park, H.-D., Noguera, D.R., 2007. Characterization of two ammonia-oxidizing bacteria isolated from reactors operated with low dissolved oxygen concentrations. J. Appl. Microbiol. 102, 1401–17. doi:10.1111/j.1365-2672.2006.03176.x

Peng, L., Ni, B.-J., Ye, L., Yuan, Z., 2015. The combined effect of dissolved oxygen and nitrite on N2O production by ammonia oxidizing bacteria in an enriched nitrifying sludge. Water Res. 73, 29–36. doi:10.1016/j.watres.2015.01.021

Petersen, B., Gernaey, K. V., Vanrolleghem, P.A., 2001. Practical identifiability of model parameters by combined respirometric-titrimetric measurements. Water Sci. Technol. 43, 347–356.

Pocquet, M., Wu, Z., Queinnec, I., Sp?randio, M., 2016. A two pathway model for N2O emissions by ammonium oxidizing bacteria supported by the NO/N2O variation. Water Res. 88, 948–959. doi:10.1016/j.watres.2015.11.029

Power, M., 1993. The predictive validation of ecological and environmental models. Ecol. Modell. 68, 33–50. doi:10.1016/0304-3800(93)90106-3

Richardson, D., Felgate, H., Watmough, N., Thomson, A., Baggs, E., 2009. Mitigating release of the potent greenhouse gas N(2)O from the nitrogen cycle - could enzymic regulation

hold the key? Trends Biotechnol. 27, 388–97. doi:10.1016/j.tibtech.2009.03.009

Rodriguez-Caballero, A., Pijuan, M., 2013. N2O and NO emissions from a partial nitrification sequencing batch reactor: exploring dynamics, sources and minimization mechanisms. Water Res. 47, 3131–40. doi:10.1016/j.watres.2013.03.019

Sayavedra-Soto, L.A., Hommes, N.G., Russell, S.A., Arp, D.J., 1996. Induction of ammonia monooxygenase and hydroxylamine oxidoreductase mRNAs by ammonium in Nitrosomonas europaea. Mol. Microbiol. 20, 541–548. doi:10.1046/j.1365-2958.1996.5391062.x

Schreiber, F., Loeffler, B., Polerecky, L., Kuypers, M.M., de Beer, D., 2009. Mechanisms of transient nitric oxide and nitrous oxide production in a complex biofilm. ISME J. 3, 1301–1313. doi:10.1038/ismej.2009.55

Schreiber, F., Wunderlin, P., Udert, K.M., Wells, G.F., 2012. Nitric oxide and nitrous oxide turnover in natural and engineered microbial communities: biological pathways, chemical reactions, and novel technologies. Front. Microbiol. 3, 372. doi:10.3389/fmicb.2012.00372

Sin, G., Gernaey, K. V, Neumann, M.B., van Loosdrecht, M.C.M., Gujer, W., 2009. Uncertainty analysis in WWTP model applications: a critical discussion using an example from design. Water Res. 43, 2894–906. doi:10.1016/j.watres.2009.03.048

Soler-Jofra, A., Stevens, B., Hoekstra, M., Picioreanu, C., Sorokin, D., van Loosdrecht, M.C.M., Pérez, J., 2016. Importance of abiotic hydroxylamine conversion on nitrous oxide emissions during nitritation of reject water. Chem. Eng. J. 287, 720–726. doi:10.1016/j.cej.2015.11.073

Spérandio, M., Pocquet, M., Guo, L., Ni, B.-J., Vanrolleghem, P.A., Yuan, Z., 2016. Evaluation of different nitrous oxide production models with four continuous long-term wastewater treatment process data series. Bioprocess Biosyst. Eng. 39, 493–510. doi:10.1007/s00449-015-1532-2

Su, Q., Ma, C., Domingo-Félez, C., Kiil, A.S., Thamdrup, B., Jensen, M.M., Smets, B.F., 2017. Low nitrous oxide production through nitrifier-denitrification in intermittent-feed high-rate nitritation reactors. Water Res. 123, 429–438. doi:10.1016/j.watres.2017.06.067

Terada, A., Lackner, S., Kristensen, K., Smets, B.F., 2010. Inoculum effects on community composition and nitritation performance of autotrophic nitrifying biofilm reactors with counter-diffusion geometry. Environ. Microbiol. 12, 2858–2872.

Yu, R., Kampschreur, M.J., van Loosdrecht, M.C.M., Chandran, K., 2010. Mechanisms and specific directionality of autotrophic nitrous oxide and nitric oxide generation during transient anoxia. Environ. Sci. Technol. 44, 1313–9. doi:10.1021/es902794a

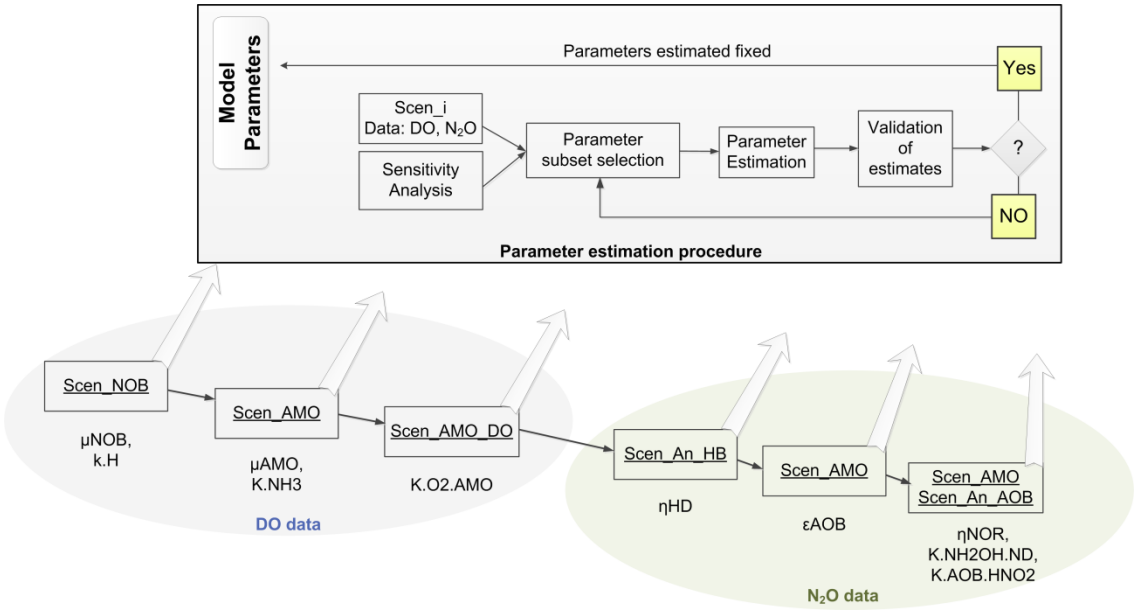

Figure 1 – Schematic of the parameter estimation procedure.

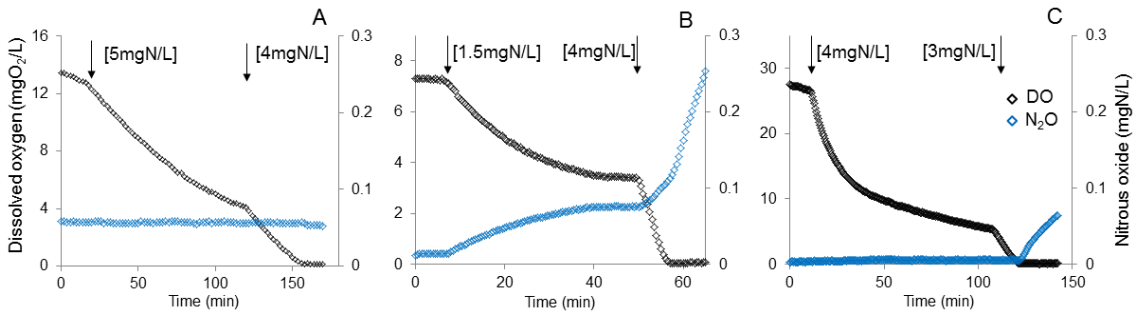

Figure 2 – Dissolved oxygen and liquid nitrous oxide concentrations during experiments: Scen_NOB (NO_2^- pulses) (A), Scen_HAO (NH_2OH pulses) (B) and Scen_AMO (NH_4^+ pulses) (C).

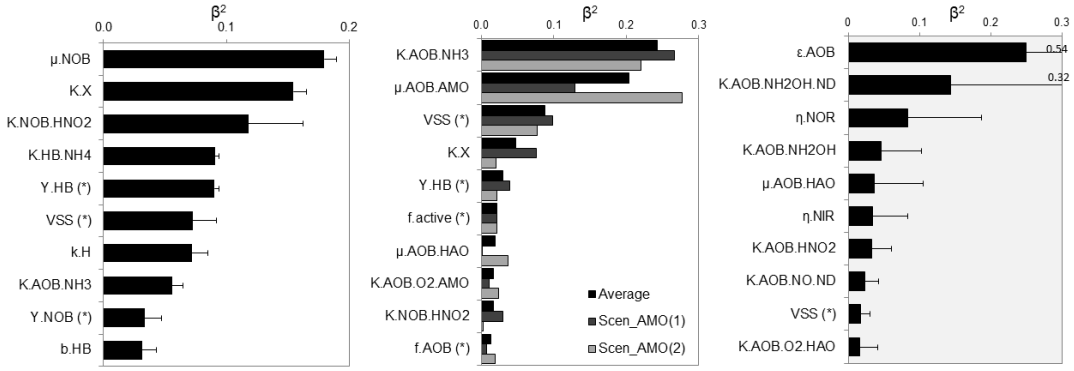

Figure 3 – Parameter sensitivity ranking of scenarios used during calibration for DO (white background) and N_2O (grey background). Scen_NOB (left), Scen_AMO (middle and right). (*) Parameters not considered for calibration. The error bars correspond to the standard deviation between experiments of the same scenario.

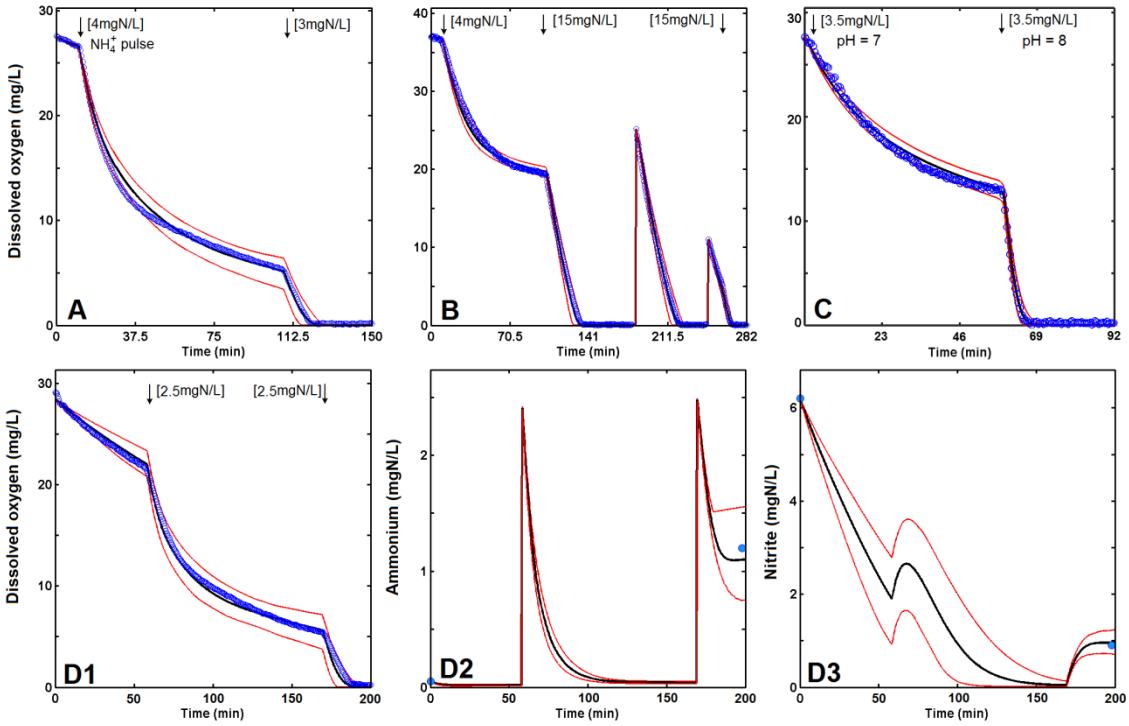

Figure 4 – Experimental DO, NH_4^+ and NO_2^- (blue markers) and model predictions (black line best-fit, red lines 95% CI). Datasets from Scen_AMO, calibration: A and B; validation: C and D.

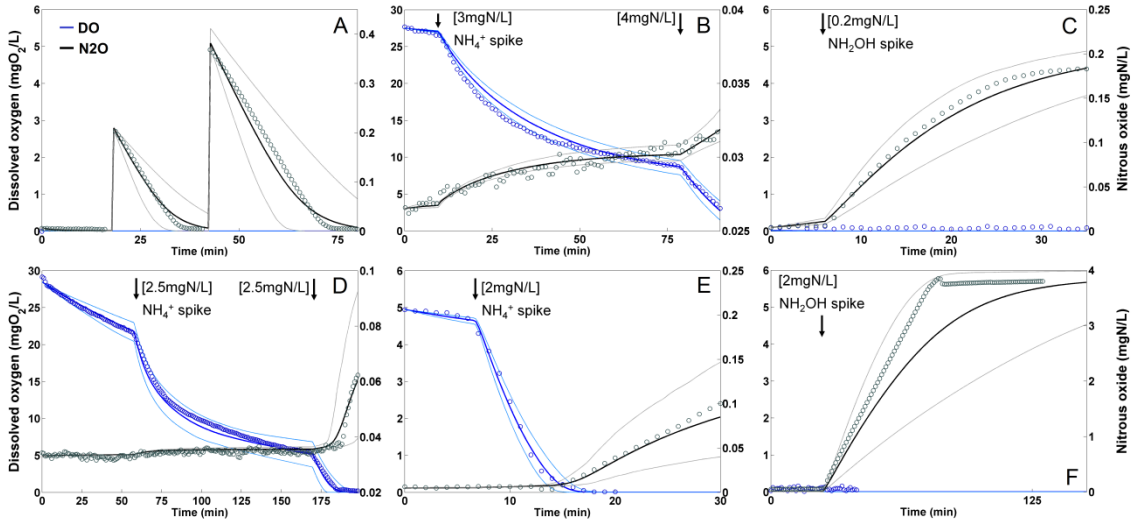

Figure 5 – Experimental N_2O (black) and DO (blue), and model predictions (dark line best-fit, light lines 95% CI) for the N_2O calibration. Datasets from calibration: (A) Scen_An_HB (N_2O pulse), (B) Scen_AMO (Aerobic NH_4^+ pulse), (C) Scen_An_AOB (Anoxic NH_2OH pulse). Datasets from validation: (D, E) Scen_AMO (Aerobic → anoxic NH_4^+ pulse), (F) Scen_An_AOB (NH_2OH pulse, excess NO_2^-).

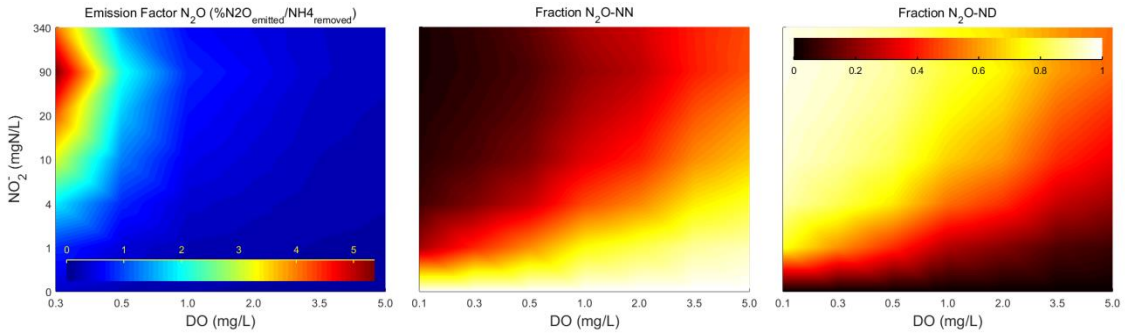

Figure 6 – Scenario analysis using the validated NHDA simulation model. Simulations were run under constant DO levels (0.1 - 0.3 - 0.5 - 1.0 - 2.0 - 3.5 - 5.0 mg/L), NO_2^- (0 – 1 – 4 – 10 – 20 – 90 – 340 mgN/L). (Left) N_2O emission factor (% N_2O/NH_4^+), colorbar: 0 – 5%, blue - red. (Middle, Right) NN, ND Pathway contribution (-), colorbar: 0 – 1, black - white.

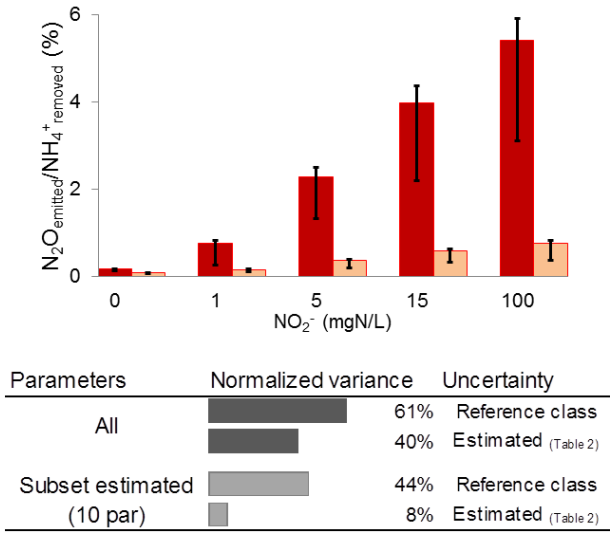

Figure 7 – Model evaluation results (500 runs) at pseudo-steady state for NH_4^+ removal at constant DO and NO_2^-: AOB-enriched biomass, pH = 7.5, NH_4^+ = 70 mgN/L, DO ([0.3 – 1.3] mg/L) and NO_2^- [0 – 1 – 5 – 15 – 100] mgN/L. (Top) N_2O emission factor at low DO (red) and high DO (light red); top standard error corresponds to uncertainty of estimated parameters only (Table 2), bottom standard error corresponds to uncertainty in All model parameters. (Bottom) Normalized variance for uncertainty considered in All model parameters (dark grey) or only for the 10 parameters estimated in this study (light grey) (Table 2) with default uncertainty (top bar) or from this study (Table 2) (bottom bar).

Table 1 – Experimental design for respirometric assays (* anoxic experiments).

Scenario	Substrate added	Targeted processes	N_2O pathways
Scen_AMO	NH_4^+	NH_4^+ removal by AOB N_2O production at excess/limiting DO (NH_4^+ excess)	NN, ND
Scen_AMO_DO	NH_4^+	Scen_AMO – Low DO	
Scen_HAO	NH_2OH	NH_2OH removal by AOB N_2O production at excess/limiting DO (NH_2OH excess)	NN, ND
Scen_NOB	NO_2^-	NO_2^- removal by NOB N_2O production at excess/limiting DO (NO_2^- excess)	HD
Scen_An_AOB*	NH_4^+, NH_2OH, NO_2^-	Role of NH_4^+, NH_2OH, NO_2^- on AOB-driven N_2O production	NN, ND
Scen_An_HB*	N_2O, NO_2^-/NO_3^-	Role of N_2O, NO_2^- and NO_3^- on HB-driven N_2O production	HD

Table 2 – Estimated parameters for each scenario (corrected for T = 20 °C). CV - coefficient of variation = variance / mean; Correlation – correlation coefficient of parameter estimates from the same scenario; RMSE – root mean squared error.

	Scenario	Parameters	Units	Best-fit	CV	Correlation		RMSE
DO data	NOB	μ_{NOB}	1/d	0.67	1.0%	1	-0.55	0.37
		k_H	1/d	2.01	0.9%	-0.55	1	
	AMO	$\mu_{AOB.AMO}$	1/d	0.49	2.0%	1	0.89	0.39
		$K_{AOB.NH3}$	mgN/L	0.12	3.9%	0.89	1	
	AMO_DO	$K_{AOB.O2.AMO}$	mgO2/L	0.23	7.0%			0.08
N_2O data	An_HB	η_{HD}	(-)	0.055	0.7%			0.03
	AMO	ε_{AOB}	(-)	0.00048	1.1%			0.001
	AMO / An_AOB	$K_{AOB.HNO2}$	µgN/L	0.67	4.4%			0.002
		η_{NOR}	(-)	0.16	3.2%	1	0.98	0.002
		$K_{AOB.NH2OH.ND}$	mgN/L	0.25	1.8%	0.98	1	